Biotransformation of Ceria Nanoparticles in Cucumber Plants

Peng Zhang,[†,#] Yuhui Ma,[†,#] Zhiyong Zhang,[†,*] Xiao He,[†] Jing Zhang,[‡] Zhi Guo,[§] Renzhong Tai,[§] Yuliang Zhao,[†] and Zhifang Chai[†]

[†]Key Laboratory for Biological Effects of Nanomaterials and Nanosafety, Key Laboratory of Nuclear Analytical Techniques, Institute of High Energy Physics, Chinese Academy of Sciences, Beijing 100049, China, [‡]Beijing Synchrotron Radiation Facility, Institute of High Energy Physics, Chinese Academy of Sciences, Beijing 100049, China, and [§]Shanghai Synchrotron Radiation Facility, Shanghai Institute of Applied Physics, Chinese Academy of Sciences, Shanghai 201204, China. [#]These authors contributed equally to this work.

ABSTRACT Biotransformation is a critical factor that may modify the toxicity, behavior, and fate of engineered nanoparticles in the environment. CeO_2 nanoparticles (NPs) are generally recognized as stable under environmental and biological conditions. The present study aims to investigate the biotransformation of CeO_2 NPs in plant systems. Transmission electron microscopy (TEM) images show needlelike clusters on the epidermis and in the intercellular spaces of cucumber roots after a treatment with 2000 mg/L CeO_2 NPs for 21 days. By using a soft X-ray scanning transmission microscopy (STXM) technique, the needlelike clusters were verified to be $CePO_4$. Near edge X-ray absorption fine structure (XANES) spectra show that Ce presented in the roots as CeO_2 and $CePO_4$ while in the shoots as CeO_2 and cerium carboxylates. Simulated studies indicate that reducing substances (*e.g.*, ascorbic acids) played a key role in the transformation process and organic acids (*e.g.*, citric acids) can promote particle dissolution. We speculate that CeO_2 NPs were first absorbed on the root surfaces and partially dissolved with the assistance of the organic acids and reducing substances excreted by the roots. The released Ce(III) ions were precipitated on the root surfaces and in intercellular spaces with phosphate, or form complexes with carboxyl compounds during translocation to the shoots. To the best of our knowledge, this is the first report confirming the biotransformation and in-depth exploring the translocation process of CeO_2 NPs in plants.

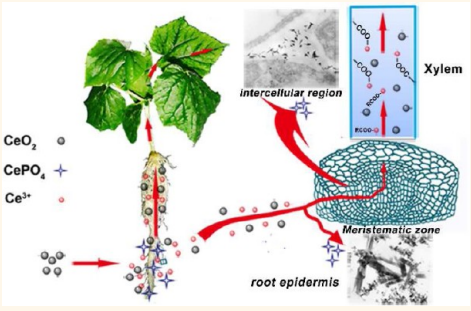

KEYWORDS: CeO_2 · $CePO_4$ · nanoparticles · plant · biotransformation

Increasing production and use of nanomaterials have raised concerns about their potential hazardous effects to the environment and human health.[1,2] Defining the behavior of nanomaterials in the environmental and biological systems is a critical research focus before aiming to understand their environmental risks.[3,4] As an essential component of the environment, plants play a crucial role in preserving the ecological equilibrium as well as providing the food sources of animals and human beings. The ongoing production and use of engineered nanoparticles (ENPs) have greatly increased the possibility of plant exposure to them, *via* an aerial or root pathway. Once adsorbed to the plant surfaces, the ENPs may be taken up, translocated, and stored in different tissues of plants, followed by being transferred to the food webs, accumulating in higher-level organisms, and causing possible biomagnifications.[5,6] Investigations on the behavior and fate of ENPs within plants are of great importance for exploring the mechanism of phytotoxicity and the full-life cycle risk assessment of ENPs.

Biotransformation, which is defined as biochemical modification by living organisms, has been studied for a long time on the common pollutants. In the process of biotransformation, either enhanced toxicity or detoxification is possible.[7] In terms of ENPs, they may also be modified by the ambient environmental media and biological systems and their final fate and toxicity to organisms may be altered.[8] Typical transformations of nanomaterials most studied recently include redox reaction, sulfidation, phosphorylation, and macromolecular/molecular modification.[9] For instance, sulfidation of Ag NPs significantly decreased their toxicity to *Escherichia coli* growth due to the lower solubility of silver sulfide.[10] Natural organic matter and humic substances absorbed on the nanoparticle surface can significantly change their aggregation state, surface properties, and toxic effects.[8,11] In the case of plants, Parsons *et al.* found the

* Address correspondence to zhangzhy@ihep.ac.cn.

Received for review August 6, 2012 and accepted October 25, 2012.

Published online October 25, 2012
10.1021/nn303543n

biotransformation of $Ni(OH)_2$ to Ni^{2+} in plant shoots and leaves while no biotransformation occurred in roots.[12] Yin *et al*. found that the silver speciation in the roots of Ag NP exposed *Lolium multiflorum* was oxidized as Ag(I).[13] A recent document reported that CuO NPs were reduced to Cu_2O and Cu_2S in maize plants.[14] We recently studied the phytotoxicity and biotransformation of two kinds of rare earth (RE) oxide nanoparticles (La_2O_3 and Yb_2O_3) in cucumber.[15,16] Root elongations of cucumber seedlings were severely inhibited by both La_2O_3 and Yb_2O_3 NPs. Biotransformation of RE oxide NPs to RE phosphates in the cucumber roots was observed. Enhanced dissolution of La_2O_3 NPs and Yb_2O_3 NPs by root-exuded organic acids was considered to play an important role in the biotransformation and phytotoxicity of them.

CeO_2 NPs have various applications including diesel fuel-borne catalyst, cosmetic additives, and polishing agent, *etc*.[17] They also have the promise to be applied as superoxide dismutase and catalase mimetics due to their electron transfer abilities.[18,19] There have been many reports on the toxicity of CeO_2 NPs to different organisms such as nematodes and bacteria.[20,21] Only a few reports pertain to the behavior of CeO_2 NPs within higher plants. By means of a radiotracer technique, Zhang *et al*. studied the uptake and distribution of two different sizes of CeO_2 NPs in cucumber plants.[22] Only a limited quantity of CeO_2 NPs could be transported from the roots to shoots. López-Moreno *et al*. found root growth was promoted by CeO_2 NPs in cucumber and corn but reduced in alfalfa and tomato. Ce speciation remained unaltered as CeO_2 NPs after uptake by roots.[23] Different biotransformations of ZnO and CeO_2 NPs in soybean were also investigated, and Zn was found only in Zn^{2+} oxidation state and was not present as ZnO NPs inside the plant, which demonstrated the biotransformation of ZnO NPs. In contrast, CeO_2 NPs did not undergo any biotransformation.[24]

According to the existing literature, no biotransformation of CeO_2 NPs occurred in plants, which was mainly due to the highly stable properties of CeO_2 NPs. Nevertheless, given that CeO_2 NPs may encounter different ambient environment across different plant species, culture media, and growth stages, the behavior and fate of CeO_2 NPs in plants would be far more complicated than the reports indicate. Our recent works have emphasized the critical role of root-excreted organic acids in enhancing the dissolution and biotransformation of rare earth oxide NPs. Therefore, we cannot ignore the potential dissolution and transformation of CeO_2 NPs in favor of plant systems.

In the present study, biotransformation of CeO_2 NPs in hydroponic cucumber plants was investigated using multiple methods. Transmission electron microscopy (TEM) was used to observe the distribution of Ce in roots of cucumber and equipped energy dispersive spectroscopy (EDS) was performed on the same regions to obtain semiquantitative information of the element composition. Speciation of Ce in the root samples were analyzed *in situ* at the cellular scale by synchrotron radiation based soft X-ray scanning transmission microscopy (STXM) technique. Chemical species of Ce in the root and shoot tissues were analyzed by means of X-ray absorption fine structure (XAFS) spectroscopy. To explore the mechanism involved in the biotransformation, we carried out a simulated study by incubating the CeO_2 NPs with four reaction solutions for 21 days and examined the transformation by infrared spectroscopy (IR) and TEM. This research will facilitate the understanding of the transformation of nanomaterials and forecasting of their fate and toxicity in the environment and biological systems.

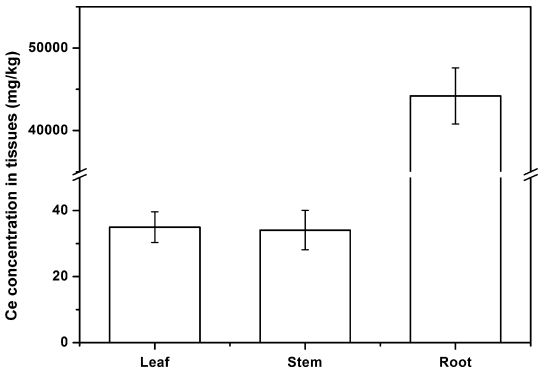

Figure 1. Ce contents in tissues of cucumber treated with CeO_2 NPs for 21 days.

RESULTS AND DISCUSSION

Ce Contents in Tissues of Cucumber. Neither CeO_2 NPs nor commercial bulk CeO_2 showed toxicity to cucumber biomass production even up to 2000 mg/L in a preexperiment (Supporting Information, Figure S2). According to the US EPA guideline (1996),[25] CeO_2 NPs can be considered as minimal toxicity on test plant species under such a high concentration. Nevertheless, distribution of CeO_2 NPs in tissues should be determined for understanding their ultimate fate in plant and environment systems. Total Ce contents in tissues of cucumber treated with 2000 mg/L were determined and the results are shown in Figure 1. The majority of Ce in the plants accumulated in the roots. Concentrations of Ce in the leaves and stems are similar.

Distribution of Cerium in the Cucumber Roots. TEM is a commonly used technique to locate the NPs in tissues. Nanoparticles with high electron density in contrast to the surrounding tissues can be easily observed and the elemental information can be obtained qualitatively and semiquantitatively by the equipped EDS. Many studies have reported the uptake and distribution of NPs in tissues observed by TEM technique.[26,27] However, up to now, there is still no report pertaining to the TEM observation of CeO_2 NPs in plant tissues. Herein, we examined the root tissues of cucumber plants by

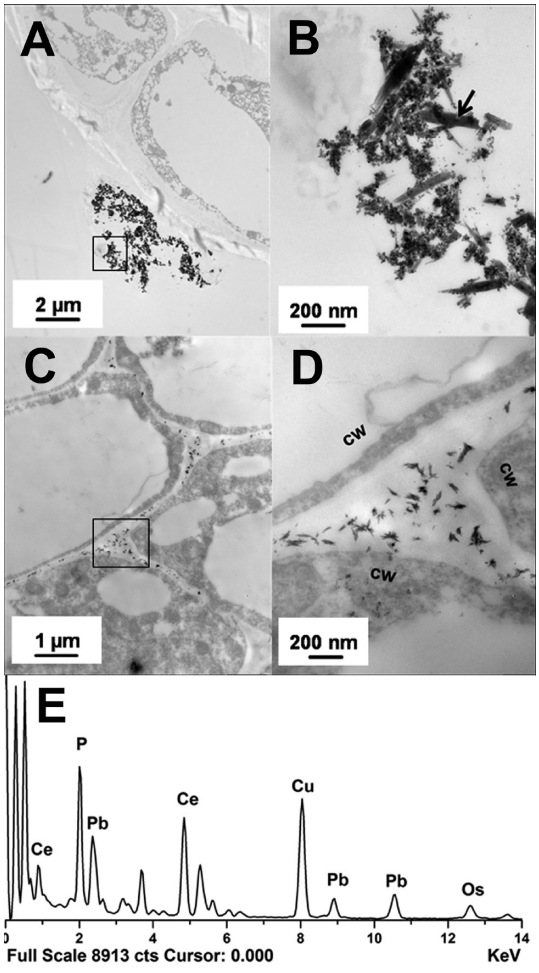

Figure 2. TEM images of the cross sections from the apical meristem region of the cucumber roots treated with 2000 mg/L CeO_2 NPs for 21 days. (A) image of the root epidermis; (C) image of the intercellular spaces; Panel B and D were respectively the magnification of the highlighted rectangle area in panels A and C; (E) EDS spectrum collected from the clusters (identified by the arrow) in panel B. cw: cell wall.

TEM and Ce-bearing particles were found in the roots. Although the roots were washed by flow tap water and deionized water for several times, a large number of CeO_2 NP agglomerates were still found on the outer epidermis (Figure 2A). This is in accordance with the previous report.[22] However, differently, except for the CeO_2 NPs, many needlelike clusters were also found mixed with the NPs (Figure 2B). We can also find a large number of needlelike clusters scattering in the intercellular regions of the root (Figure 2C,D). To determine the elemental composition of these clusters, an EDS spot-scanning technique was performed on clusters both on the root epidermis (Figure 2E) and in the intercellular regions (figure not shown). The atomic ratio of Ce/P was close to 1, indicating the composition of these clusters may be $CePO_4$. It is well-known that RE^{3+} ions can be easily captured by PO_4^{3-} and form insoluble $REPO_4$ (solubility product = 10^{-24}–10^{-26}).[28] It is reported that the sorbed Ce^{3+} ions on the cell surface of *Saccharomyces cerevisiae* can react with PO_4^{3-} released from inside the yeast cells and form the Ce(III) phosphates nanocrystallites.[29] Phosphate anions may also bind with the surface cerium(III) of CeO_2 NPs and form $CePO_4$, resulting in the shift of the SOD activity and the catalase mimetic activity of CeO_2 NPs.[30] Although the existing literatures and EDS results show the possibility that these needlelike clusters in our results might be $CePO_4$, to confirm it, it is still necessary to further identify their chemical species.

***In Situ* Speciation of Cerium in the Roots.** STXM is a powerful technique to map the chemical composition *in situ* at cellular level with high spatial resolution of better than 30 nm. Chemical mappings of RE compounds ($LaPO_4$ and $YbPO_4$) in plant cells using STXM have been reported recently.[15,16] In the present work, cross sections of 1.5 μm thickness adjacent to those for TEM observation were chosen for STXM stack analysis to obtain the spatial distribution of Ce-components. Ce distributions on root epidermis and in intercellular regions were proved by dual energy analysis (Figure 3B and F). Stack analyses were then applied on these Ce distributing region and presented as a color-coded map (Figure 3C,G). Near edge X-ray absorption fine structure (XANES) spectra (Figure 3D) extracted from the color-coded map on the root epidermis (Figure 3C) clearly exhibit a mixture of characteristic peaks of $CePO_4$ and CeO_2. While in intercellular spaces, the red color spectrum (Figure 3H), which was extracted from the red particles in the color-coded map (Figure 3G), shows exactly the same feature as $CePO_4$. Combining these results with the TEM/EDS results, we substantiated that these needlelike clusters on root epidermis and in intercellular spaces are $CePO_4$. There are several types of NPs that have been proved to be transformed in plants.[12,24] However, in the case of CeO_2 NPs, there is still no direct evidence on the biotransformation of them in biological systems to date. Although several reports claimed that CeO_2 NPs underwent valence change and transformation, unfortunately, there was a lack of sufficient evidence to prove the presence and the chemical composition of the transformation products.[30,31] To the author's knowledge, this is the first report confirming the biotransformation of CeO_2 NPs and determining the transformation products.

Speciation Analysis of Cerium in the Cucumber Plants by XANES. Because of the low content of Ce in leaf and stem tissues, it is hard to find the CeO_2 or Ce-bearing particles in the places of interest and thus *in situ* detection by TEM or STXM is difficult. Therefore, synchrotron radiation based XANES technique was applied to determine Ce speciation in the roots, stems and leaves.

XANES at the L_{III} threshold has been the most powerful method to determine the valence of REs.[32] Normalized Ce-L_{III}-edge XANES spectra of standard compounds and cucumber samples were shown in Figure 4. Three typical features can be found from the

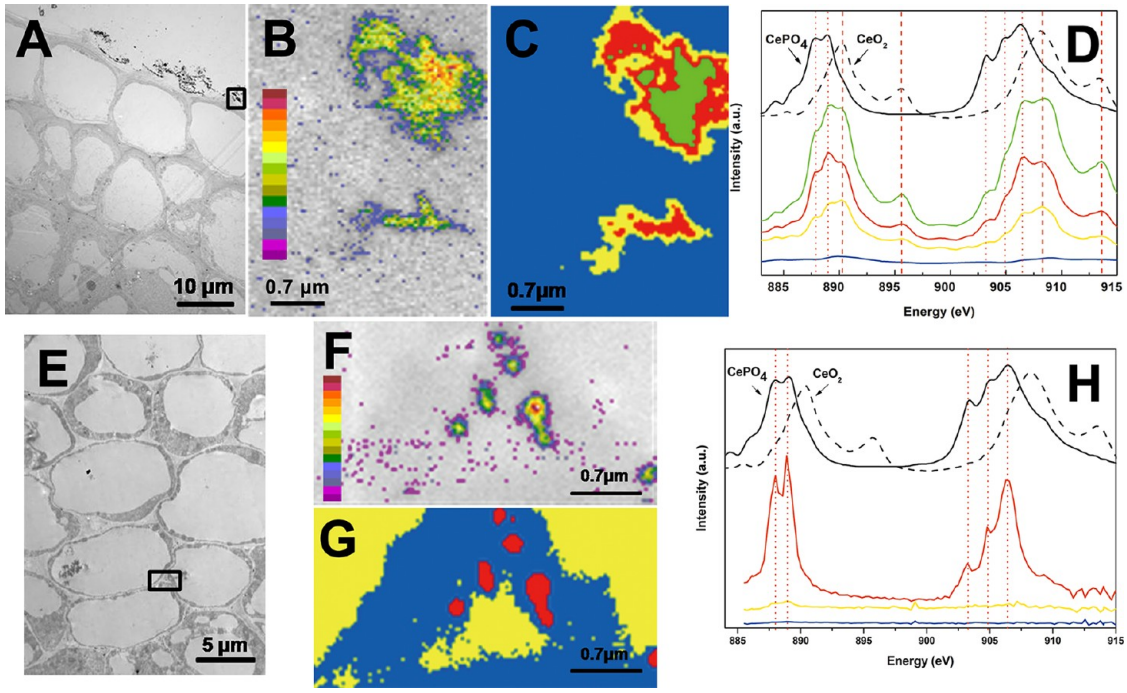

Figure 3. (A and E): TEM images of root cells; (B and F): Ce maps of rectangle area in panels A and E obtained by a ratio of 886 and 888 eV images. Color bar values are estimated from Ce absorption coefficients and X-ray absorption measurements (in g/cm^2). The calculated surface densities are respectively between 1.1×10^{-5} to 6.4×10^{-5} g/cm^2 and 2.4×10^{-6} to 2.8×10^{-5} g/cm^2; (C and G): color-coded maps of Ce-components in panels B and F derived from an STXM Ce M edge stack analysis. The order of Ce contents is as follows: green > red > yellow; blue color represents the non-Ce regions; Panels D and H are respectively the XAFS spectra extracted from the image sequences of panels C and G. The black line spectra above belong to the standard compounds and the colored spectra below belong to the root samples. The vertical red dotted lines indicate the characteristic peaks of $CePO_4$ and the dash lines indicate the characteristic peaks of CeO_2 NPs.

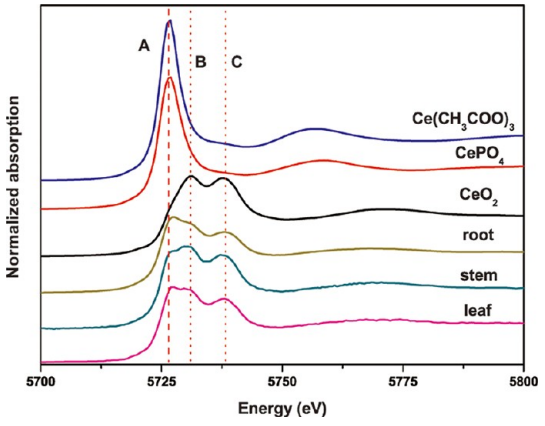

Figure 4. XANES Ce L_{III}-edge spectra (5723 eV) of root, stem, and leaf of cucumber plants treated with 2000 mg/L CeO_2 NPs for 21 days. Vertical dash line and dotted line marked the feature of Ce(III) and Ce(IV) compounds, respectively.

spectra which are respectively the low energy feature A and the high energy feature B and C. Feature A is attributed to the characteristic peak of Ce(III) oxidation state such as $CePO_4$ and $Ce(NO_3)_3$ herein. The feature B and C, which are described as mixing of multielectron configurations $4f^0L$ and $4f^1L$, are the characteristic peaks of Ce(IV) oxides and compounds.[33] This spectral difference is an important criterion for distinguishing Ce compounds of the two different oxidation states. In the root samples, the spectra obviously exhibit a mixture of features B and C. Compared with the spectra of standard compounds, the feature B in the spectra of roots merged into feature A and almost disappeared. This indicates the coexistence of Ce(III) and Ce(IV) oxidation states in the root samples, which sufficiently proves that Ce(IV) of CeO_2 NPs was partially reduced to Ce(III). Ce oxidation state in the leaves and stems were also examined by XANES. Despite of the noise disturbance in the spectra of the leaves and stems due to the low Ce contents, we can also see from the XANES spectra that both Ce(III) and Ce(IV) oxidation states existed and the spectra are similar to that of the roots. To obtain the quantitative information of the Ce speciation, linear combination fitting (LCF) was performed on the normalized XANES spectra using CeO_2, $CePO_4$, and $Ce(CH_3COO)_3$ as the reference compounds. Herein, we choose $Ce(CH_3COO)_3$ as the representation of cerium carboxylates which possibly formed in plants. The fitting spectra and parameters indicate that the fitting results are satisfying and convincible (Supporting Information, Figure S3). LCF results show that Ce species in the roots presented as 66% CeO_2 and 34% $CePO_4$. However, Ce species presented in the stems as 86.4% CeO_2 and 13.6% cerium carboxylates, and in the leaves as 78.5% CeO_2 and 21.5% cerium carboxylates. These results suggest that part of the CeO_2 NPs were transformed

to Ce(III) species in the whole plants. It should be noted that the quantitative information in the roots may not reflect the absolute component proportion due to uncertainty of the washing process. But the clear difference that can be seen is that Ce(III) speciation exhibits as $CePO_4$ in roots while as cerium carboxylates in stems and leaves. Roots were abundant in PO_4^{3-} because they were completely immersed in the nutrient solution. Most of the released Ce^{3+} was precipitated as insoluble $CePO_4$ and immobilized in the roots. A small part of the Ce^{3+} may be transported with CeO_2 NPs to the shoots *via* the water flow and complexed by carboxyl-containing substances.[34] CeO_2 NPs accounted for the most proportion of Ce species in the leaves and stems. These results confirm the biotransformation of CeO_2 NPs and provide direct evidence of the translocation of CeO_2 NPs and the transformed products from the roots to shoots. It is possible that the CeO_2 NPs may also be transformed to Ce(III) in plants. Further studies are required to validate this hypothesis. The residual materials in the exposure solution at the end of the growth period were also analyzed by XANES (Supporting Information, Figure S4). The spectrum shows the same feature as the CeO_2. LCF analysis shows that the residual materials were composed of 97.2% CeO_2 and 2.7% $CePO_4$, which indicates that most of the CeO_2 NPs in the exposure solution remained unaltered. This indirectly suggests that most of the transformation of CeO_2 occurred on the root surface rather than in the exposure solution.

Transformation of CeO_2 NPs by Simulated Studies. Transformation of nanoparticles either chemically or biologically may alter their behavior and toxicity in the environment. The factors that affect the transformation in the biological system are complicated. Redox potential of the ambient environment will play an important role in the transformation of NPs which are composed of elements with changeable valences. Natural water and aerated soil are always in an oxidizing environment, while a hydroponic system and nonaerated soil such as a wetland are predominantly in a reducing environment.[9,35] Additionally, plants can produce reducing substances such as reducing sugars and phenols which will result in redox reactions.[14]

Microbes surrounding the plant roots can also produce abundant reducing substances in their metabolic processes.[36] In the present study, CeO_2 underwent the valence change from Ce(IV) to Ce(III), therefore, it is reasonable to consider that reducing agents would be a critical factor involved in the transformation. In addition, dissolution of nanoparticles is also an important step in the transformation process. Factors stimulating the dissolution will undoubtedly promote the transformation of nanoparticles. Biogenic organic acids have been suggested to be an important factor which may stimulate the biotransformation of nanoparticles in plants.[15,16] Plant roots can create a microenvironment

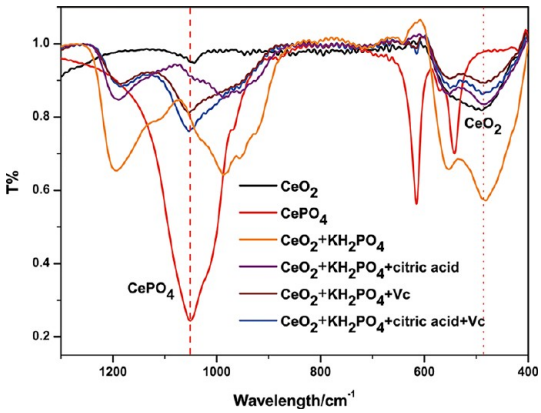

Figure 5. IR spectra of CeO_2 NPs incubated in different media for 21 d.

around the roots called a rhizosphere by secreting large quantities of substances including organic acids. Therefore, we consider that CeO_2 NPs might be reduced first and released as Ce^{3+} with the assistance of reducing substances and organic acids, and then the Ce^{3+} was precipitated with PO_4^{3-} or complexed by the carboxylates.

On the basis of the hypothesis above, simulated transformations of CeO_2 NPs in different aqueous media were examined. The IR spectra of the products were shown in Figure 5. After incubation in a solution composed of KH_2PO_4 or KH_2PO_4 + citric acid for 21 days, the spectra show a clear broad peak at 490 cm^{-1} that belongs to CeO_2 NPs. Features at 1185 and 980 cm^{-1} are attributed to $\nu_s PO_2$ and $\nu P{-}OH$ and no typical features of $\nu_{as} PO_2$ in $CePO_4$ at 1043 cm^{-1} were observed. These suggest that $H_2PO_4^-$ or HPO_4^{2-} were absorbed on the surface of CeO_2 NPs but no $CePO_4$ was formed. When the incubation solution contained ascorbic acids (Vc), the feature at 1043 cm^{-1} appeared and the peak intensity at 490 cm^{-1} decreased compared to that in the solutions without Vc. These indicate the reduction of CeO_2 NPs and the formation of $CePO_4$. Additionally, comparing the peak intensity at 1043 cm^{-1}, we can see that citric acid promoted the formation of $CePO_4$. More evidence were further provided by TEM images as shown in Figure 6. In the treatment without Vc, CeO_2 NPs remained in the pristine crystal form (Supporting Information, Figure S5A). When cultured in media KH_2PO_4 + Vc, dendritic crystals appeared (Figure 6A). HRTEM results show clear (111) and (100) fringe lattices with the interplanar spacings of 0.31 and 0.61 nm, which are respectively attributed to cubic phase CeO_2 and hexagonal phase $CePO_4$ (Figure 6B). When incubated in KH_2PO_4 + citric acid + Vc, more dendritic crystals with large quantities of adsorbed and embedded CeO_2 NPs were observed (Figure 6C). As seen from the HRTEM image (Figure 6D), interplanar spacings of 0.61 and 0.43 nm are attributed to (100) and (101) fringe lattices of $CePO_4$. Clear fringe lattices (111) and (002) which are attributed to CeO_2

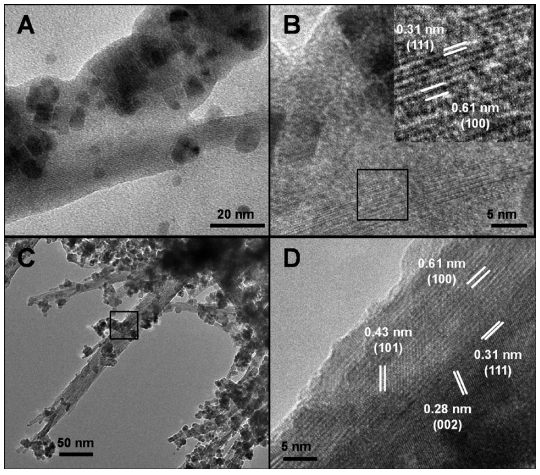

Figure 6. TEM images of CeO_2 NPs incubated in media KH_2PO_4 + Vc (A) and KH_2PO_4 + citric acid + Vc (C). Panels B and D were magnification of the rectangle areas in panels A and C.

can also be found. In addition, the (111) and (100) planes are along the same direction, and we found many dendritic crystals with the (111) plane but with larger size than pristine CeO_2 NPs (Supporting Information, Figure S5B). These suggest that CeO_2 NPs may assemble along the (111) plane and grow to $CePO_4$ ultimately. The results above suggest that a reducing substance is a critical factor resulting in the biotransformation of CeO_2 NPs. Organic acids can stimulate the continuous dissolution of CeO_2 NPs.

Commercial CeO_2 NPs were also studied and similar clusters on the root epidermis were observed (Supporting Information, Figure S6A–D). EDS was also performed on the clusters and the results were similar to that of 7 nm CeO_2 NPs, while the difference is that the number of transformed CeO_2 NPs was relatively less than that of the 7 nm CeO_2 NPs and no clusters can be found in the intercellular spaces for the commercial CeO_2 NPs treated cucumber plants. This may be due to the different physicochemical properties (*e.g.*, size, chemical reactivity, *etc.*) of the commercial CeO_2 NPs. We also examined the biotransformation of CeO_2 in other plants. TEM images of the roots of soybean treated with 7 nm CeO_2 NPs were shown in Supporting Information, Figure S7. Similar needlelike clusters were observed on the root surfaces and in the intercellular spaces (Figure S7), indicating that the biotransformation can occur in different plant species.

CeO_2 NPs are always used as the insoluble model material to study the behavior of nanoparticles in biological or environmental systems and compared with other soluble nanomaterials such as ZnO NPs.[37] Phosphates widely exist in environmental and biological systems and are the base components of the buffer solution in laboratory researches. Organic acids also have wide distribution in the environment and plants. For instance, concentration of oxalic acid and citric acid in plant cells and tissues can be as high as 1 mM.[38] In addition, plants can produce many reducing substances such as catechol and reducing sugars. Given that, CeO_2 NPs may undergo biotransformation when in contact with biogenic reducing substances with the assistance of PO_4^{3-} and organic acids, then their ultimate fate and toxicity may be changed. Therefore, data regarding toxicity of pristine CeO_2 NPs are not informative enough. Seen from our results, more complicated interactions between nanoparticles and the biological systems should be recognized and the feasibility of using CeO_2 NPs as the representative insoluble nanomaterial should be reassessed. Transformation, ultimate fate, and toxicity of nanoparticles in both ambient media and biological systems should be detailed addressed in future studies.

CONCLUSION

CeO_2 NPs with high stability can undergo biotransformation in plant systems. Biogenic reducing substances and organic acids as well as PO_4^{3-} may be the key factors involved in the biotransformation process. The results presented in this manuscript highlight the importance of the biological system in the transformation of nanoparticles. The modification of nanoparticles in the transformation will not only change their fate and toxicity, but also may cause dysfunction of their beneficial application such as delivery systems and imaging agents for plants. Therefore, the mechanisms and extent of these transformations should be addressed in future studies not only for the risk assessment but also for the proper application of nanoparticles.

MATERIALS AND METHODS

Synthesis and Characterization of CeO_2 NPs. CeO_2 NPs were synthesized by a precipitation method as described in a previous literature.[22] The particle shape and structure were assessed by TEM (JEM 200CX, Japan) and XRD (X'pert PRO MPD, Holland). The TEM image shows that the NPs present a truncated octahedral shape with an average size of 6.9 ± 0.4 nm (Supporting Information, Figure S1A). The XRD pattern indicates that the peaks can be indexed to pure fluorite cubic structure (Figure S1B). Particle size and zeta potential of the CeO_2 NPs (a suspension of 20 mg/L) were assessed by a Nicomp 380 ZLS Zeta potential/Particle system (PSS Nicomp, Santa Barbara, CA, USA). Hydrodynamic sizes of the CeO_2 NPs in deionized water and the nutrient solution are 40.2 ± 7.2 nm and 691.7 ± 26 nm, respectively. Zeta potentials of the CeO_2 NPs in deionized water and the nutrient solution are 32.9 ± 8.5 mV and −15.1 ± 3.5 mV, respectively.

Seedling Culture and Nanoparticles Application. Cucumber seeds were purchased from Chinese Academy of Agricultural Sciences. Seeds were immersed in 10% NaClO solution for 10 min, followed by a rinse with deionized water to ensure the surface sterility. Then the seeds were arrayed in Petri dishes with moist filter papers and placed in the dark in an artificial climatic chamber

at 25 °C. After 3 days incubation, uniform seedlings were selected and each seedling was anchored by a plastic foam with a hole and transferred into a 250 mL beaker containing 100 mL of modified 1/4 strength Hogland solution. Six replicates were set. The seedlings were allowed to grow in a growth chamber (PRX-450C, Saifu, China) with a day/night temperature of 27 °C/18 °C, day/night humidity of 50%/70% and 16 h photoperiod (light intensity of 1.76×10^4 lux) for 10 days before treatment. CeO_2 NPs were then added into the nutrient solution to a concentration of 2000 mg/L followed by ultrasonic pretreatment for 15 min. The seedlings were placed in the growth chamber and allowed to grow for three weeks. The solution in each beaker was replenished to maintain a constant volume (100 mL) with fresh nutrient solution every other day.

Ce Contents Determination by ICP−MS. At the end of the growth period, the seedlings were harvested and washed thoroughly with deionized water, and then lyophilized with a freeze-dryer. Roots and shoots were separated and weighed. The dry samples were ground to fine powders and digested with a mixture of HNO_3 and H_2O_2 on a heating plate. Total Ce contents in the plant tissues were measured by ICP−MS.

Transmission Electronic Microscopy Observation and Energy Dispersive Spectroscopy. After a 21 d treatment, cucumber roots were washed with deionized water thoroughly and the root apexes were cut and fixed in 2.5% glutaraldehyde solution. Then they were dehydrated in a graded acetone series and embedded in Spurr's resin. Ultrathin sections (90 nm) were obtained using an UC6i ultramicrotome (Leica, Austria) with a diamond knife. The sections were collected on copper grids followed by staining with uranyl acetate and lead citrate and observed on a JEM-1230 (JEOL, Japan) transmission electron microscope operating at 80 kV. TEM/EDS spectra were collected on a TEM (Oxford Instruments, Oxfordshire, UK) equipped with energy dispersive X-ray spectrometer with a beam diameter of 25 nm. More than 10 sections cut from different roots were examined.

Soft X-ray Scanning Transmission Microscopy. Ce $M_{4,5}$ edges X-ray absorption near edge structure (XANES) measurements and STXM imaging were performed at the beamline BL08U1 of the Shanghai Synchrotron Radiation Facility. CeO_2 NPs, $CePO_4$, $Ce(NO_3)_3 \cdot 6H_2O$ as well as $Ce(CH_3COO)_3 \cdot 6H_2O$ were chosen as the standard materials. The standard materials were ultrasonically dispersed in ethanol and deposited on a TEM grid. Samples of root sections with a thickness of 1.5 μm were prepared by the protocols as described in the process of TEM sample preparation. The grids were fixed on a sample holder and loaded into the experimental chamber. First, a dual-energy method was performed on the chosen regions of the sample and a Ce-element map was derived by calculation to ensure the existence of the Ce-component in the regions. Then, image sequences (called "stack") were acquired at multiple energies spanning the relevant element absorption edge (from 884 to 915 eV for Ce $M_{4,5}$ edge). Then they were aligned *via* a spatial cross-correlation analysis method. Finally, XANES spectra were extracted from groups of pixels that have similar absorption features within the image region of interest using the IDL package aXis2000.

X-ray Absorption Spectroscopy. Samples of cucumber treated with 2000 mg/L CeO_2 NPs were collected and washed thoroughly with deionized water at the end of experiment. Leaves, stems, and roots were separated and lyophilized with a freeze-dryer. The dried samples were motor homogenized and pressed into thin slices with diameter of 10 mm and thickness of 2 mm. XAS spectra were collected on beamline 1W1B at Beijing Synchrotron Radiation Facility. The ring storage energy of the synchrotron radiation accelerator during data collection was 2.5 GeV with current intensity of 50 mA. Ce L_{III}-edge spectrum of the root sample was collected using transmission mode. Fluorescence mode was applied for collection of Ce L_{III}-edge spectra of stems and leaves using a 19-element germanium array solid detector. $CePO_4$ and $Ce(CH_3COO)_3$ as well as CeO_2 NPs were used as standard compounds. Athena software was used to process the normalization and liner combination fitting (LCF) of the XANES spectra. At the end of growth period, the exposure solutions were lyophilized after the plants were harvested and analyzed by XANES.

Simulation Studies on the Biotransformation of CeO_2 NPs. Four reaction solutions, which separately were composed of KH_2PO_4, KH_2PO_4 + citric acid, KH_2PO_4 + ascorbic acid (Vc), and KH_2PO_4 + citric acid + Vc, were prepared. The final concentrations of all the components were set as 1 mM, and the pH values were adjusted to 5.5 which were same as that of the nutrient solution. CeO_2 NPs were added to the solutions with stirring and ultrasonication. The final concentrations of CeO_2 NPs in the suspensions were 200 and 2000 mg/L. After a 21 d static incubation, the 2000 mg/L suspensions were centrifuged and washed with deionized water for three times. The pellets were lyophilized under −50 °C, quantitatively mixed with KBr and finely grinded and pressed into transparent slices. The infrared spectra (IR) were recorded on an IR spectrometer (Tensor 27, Bruker, Germany) in the wavenumber range of 400−4000 cm^{-1}. The CeO_2 NPs suspensions of 200 mg/L in the series of reaction solutions were used for TEM observation.

Conflict of Interest: The authors declare no competing financial interest.

Supporting Information Available: TEM image and XRD pattern of CeO_2 NPs (Figure S1); biomass of cucumber treated with nanoparticulate and bulk CeO_2 (Figure S2); LCF results of Ce XANES normalized spectra of cucumber root, leaf and stem (Figure S3); XANES Ce L_{III}-edge normalized spectra of the residual material in the exposure solution at the end of the growth period (Figure S4); HRTEM images of CeO_2 NPs incubated in KH_2PO_4 and KH_2PO_4 + Vc (Figure S5); TEM images of cucumber roots treated with commercial CeO_2 NPs (Figure S6); TEM images of roots of soybean treated with 7 nm CeO_2 NPs (Figure S7). This material is available free of charge *via* the Internet at http://pubs.acs.org.

Acknowledgment. This work was financially supported by the Ministry of Science and Technology of China (Grant No. 2011CB933400, 2013CB932703), Ministry of Environmental Protection of China (Grant No. 201209012) and National Natural Science Foundation of China (Grant No. 10905062, 11005118, 11275215, 11275218).

REFERENCES AND NOTES

1. Nel, A.; Xia, T.; Mädler, L.; Li, N. Toxic Potential of Materials at the Nanolevel. *Science* **2006**, *311*, 622–627.
2. Handy, R. D.; Owen, R.; Valsami-Jones, E. The Ecotoxicology of Nanoparticles and Nanomaterials: Current Status, Knowledge Gaps, Challenges, and Future Needs. *Ecotoxicology* **2008**, *17*, 315–325.
3. Maynard, A.; Aitken, R. J.; Butz, T.; Colvin, V.; Donaldson, K.; Oberdörster, G.; Philbert, M. A.; Ryan, J.; Seaton, A.; Stone, V. Safe Handling of Nanotechnology. *Nature* **2006**, *444*, 267–269.
4. Nel, A. E.; Mädler, L.; Velegol, D.; Xia, T.; Hoek, E. M. V.; Somasundaran, P.; Klaessig, F.; Castranova, V.; Thompson, M. Understanding Biophysicochemical Interactions at the Nano-Bio Interface. *Nat. Mater.* **2009**, *8*, 543–557.
5. Holbrook, R. D.; Murphy, K. E.; Morrow, J. B.; Cole, K. D. Trophic Transfer of Nanoparticles in a Simplified Invertebrate Food Web. *Nat. Nanotechnol.* **2008**, *3*, 352–355.
6. Judy, J. D.; Unrine, J. M.; Bertsch, P. M. Evidence for Biomagnification of Gold Nanoparticles within a Terrestrial Food Chain. *Environ. Sci. Technol.* **2011**, *45*, 776–781.
7. Abramowicz, D. A. Aerobic and Anaerobic Biodegradation of PCBs: A Review. *Crit. Rev. Biotechnol.* **1990**, *10*, 241–251.
8. Van Hoecke, K.; De Schamphelaere, K. A. C.; Van der Meeren, P.; Smagghe, G.; Janssen, C. R. Aggregation and Ecotoxicity of CeO_2 Nanoparticles in Synthetic and Natural Waters with Variable pH, Organic Matter Concentration and Ionic Strength. *Environ. Pollut.* **2011**, *159*, 970–976.
9. Lowry, G. V.; Gregory, K. B.; Apte, S. C.; Lead, J. R. Transformations of Nanomaterials in the Environment. *Environ. Sci. Technol.* **2012**, *46*, 6893–6899.
10. Reinsch, B. C.; Levard, C.; Li, Z.; Ma, R.; Wise, A.; Gregory, K. B.; Brown, G. E.; Lowry, G. V. Sulfidation of Silver Nanoparticles Decreases *Escherichia coli* Growth Inhibition. *Environ. Sci. Technol.* **2012**, *46*, 6992–7000.

11. Fabrega, J.; Fawcett, S. R.; Renshaw, J. C.; Lead, J. R. Silver Nanoparticle Impact on Bacterial Growth: Effect of pH, Concentration, and Organic Matter. *Environ. Sci. Technol.* **2009**, *43*, 7285–7290.
12. Parsons, J. G.; Lopez, M. L.; Gonzalez, C. M.; Peralta-Videa, J. R.; Gardea-Torresdey, J. L. Toxicity and Biotransformation of Uncoated and Coated Nickel Hydroxide Nanoparticles on Mesquite Plants. *Environ. Toxicol. Chem.* **2010**, *29*, 1146–1154.
13. Yin, L.; Cheng, Y.; Espinasse, B.; Colman, B. P.; Auffan, M.; Wiesner, M.; Rose, J.; Liu, J.; Bernhardt, E. S. More than the Ions: The Effects of Silver Nanoparticles on *Lolium multiflorum*. *Environ. Sci. Technol.* **2011**, *45*, 2360–2367.
14. Wang, Z.; Xie, X.; Zhao, J.; Liu, X.; Feng, W.; White, J. C.; Xing, B. Xylem-and Phloem-Based Transport of CuO Nanoparticles in Maize (*Zea mays* L.). *Environ. Sci. Technol.* **2012**, *46*, 4434–4441.
15. Ma, Y.; He, X.; Zhang, P.; Zhang, Z.; Guo, Z.; Tai, R.; Xu, Z.; Zhang, L.; Ding, Y.; Zhao, Y. Phytotoxicity and Biotransformation of La_2O_3 Nanoparticles in a Terrestrial Plant Cucumber (*Cucumis sativus*). *Nanotoxicology* **2011**, *5*, 743–753.
16. Zhang, P.; Ma, Y.; Zhang, Z.; He, X.; Guo, Z.; Tai, R.; Ding, Y.; Zhao, Y.; Chai, Z. Comparative Toxicity of Nanoparticulate/Bulk Yb_2O_3 and $YbCl_3$ to Cucumber (*Cucumis sativus*). *Environ. Sci. Technol.* **2012**, *46*, 1834–1841.
17. Cassee, F. R.; Van Balen, E. C.; Singh, C.; Green, D.; Muijser, H.; Weinstein, J.; Dreher, K. Exposure, Health and Ecological Effects Review of Engineered Nanoscale Cerium and Cerium Oxide Associated with Its Use as a Fuel Additive. *Crit. Rev. Toxicol.* **2011**, *41*, 213–229.
18. Heckert, E. G.; Karakoti, A. S.; Seal, S.; Self, W. T. The Role of Cerium Redox State in the SOD Mimetic Activity of Nanoceria. *Biomaterials* **2008**, *29*, 2705–2709.
19. Pirmohamed, T.; Dowding, J. M.; Singh, S.; Wasserman, B. W. B.; King, J.; Heckert, E.; Karakoti, A. S.; King, J. E. S.; Seal, S.; Self, W. T. Nanoceria Exhibit Redox State-Dependent Catalase Mimetic Activity. *Chem. Commun.* **2010**, *46*, 2736–2738.
20. Kuang, Y.; He, X.; Zhang, Z.; Li, Y.; Zhang, H.; Ma, Y.; Wu, Z.; Chai, Z. Comparison Study on the Antibacterial Activity of Nano-or Bulk-Cerium Oxide. *J. Nanosci. Nanotechnol.* **2011**, *11*, 4103–4108.
21. Zhang, H.; He, X.; Zhang, Z.; Zhang, P.; Li, Y.; Ma, Y.; Kuang, Y.; Zhao, Y.; Chai, Z. Nano-CeO_2 Exhibits Adverse Effects at Environmental Relevant Concentrations. *Environ. Sci. Technol.* **2011**, *45*, 3725–3730.
22. Zhang, Z.; He, X.; Zhang, H.; Ma, Y.; Zhang, P.; Ding, Y.; Zhao, Y. Uptake and Distribution of Ceria Nanoparticles in Cucumber Plants. *Metallomics* **2011**, *3*, 751–854.
23. López-Moreno, M. L.; de la Rosa, G.; Hernández-Viezcas, J. A.; Peralta-Videa, J. R.; Gardea-Torresdey, J. L. X-ray Absorption Spectroscopy (XAS) Corroboration of the Uptake and Storage of CeO_2 Nanoparticles and Assessment of Their Differential Toxicity in Four Edible Plant Species. *J. Agr. Food. Chem.* **2010**, *58*, 3689–3693.
24. López-Moreno, M. L.; de la Rosa, G.; Hernández-Viezcas, J. A.; Castillo-Michel, H.; Botez, C. E.; Peralta-Videa, J. R.; Gardea-Torresdey, J. L. Evidence of the Differential Biotransformation and Genotoxicity of ZnO and CeO_2 Nanoparticles on Soybean (*Glycine max*) Plants. *Environ. Sci. Technol.* **2010**, *44*, 7315–7320.
25. U.S. EPA. Ecological effects test guidelines. OPPTS 850.4150 Terrestrial Plant Toxicity, Tier I (vegetative Vigor); EPA 712-C-96-163; Public Draft. Office of Prevention, Pesticides and Toxic Substances: Washington, DC, 1996.
26. Lee, W. M.; An, Y. J.; Yoon, H.; Kweon, H. S. Toxicity and Bioavailability of Copper Nanoparticles to the Terrestrial Plants Mung Bean (*Phaseolus radiatus*) and Wheat (*Triticum aestivum*): Plant Agar Test for Water-Insoluble Nanoparticles. *Environ. Toxicol. Chem.* **2008**, *27*, 1915–1921.
27. Corredor, E.; Testillano, P. S.; Coronado, M. J.; González-Melendi, P.; Fernández-Pacheco, R.; Marquina, C.; Ibarra, M. R.; De La Fuente, J. M.; Rubiales, D.; Pérez-de-Luque, A. Nanoparticle Penetration and Transport in Living Pumpkin Plants: *in Situ* Subcellular Identification. *BMC Plant Biol.* **2009**, *9*, 45.
28. Byrne, R. H.; Kim, K. H. Rare Earth Precipitation and Coprecipitation Behavior: The Limiting Role of PO_4^{3-} on Dissolved Rare Earth Concentrations in Seawater. *Geochim. Cosmochim. Acta* **1993**, *57*, 519–526.
29. Jiang, M.; Ohnuki, T.; Kozai, N.; Tanaka, K.; Suzuki, Y.; Sakamoto, F.; Kamiishi, E.; Utsunomiya, S. Biological Nano-mineralization of Ce Phosphate by *Saccharomyces cerevisiae*. *Chem. Geol.* **2010**, *277*, 61–69.
30. Singh, S.; Dosani, T.; Karakoti, A. S.; Kumar, A.; Seal, S.; Self, W. T. A Phosphate-Dependent Shift in Redox State of Cerium Oxide Nanoparticles and Its Effects on Catalytic Properties. *Biomaterials* **2011**, *32*, 6745–6753.
31. Thill, A.; Zeyons, O.; Spalla, O.; Chauvat, F.; Rose, J.; Auffan, M.; Flank, A. M. Cytotoxicity of CeO_2 Nanoparticles for *Escherichia coli*. Physico-chemical Insight of the Cytotoxicity Mechanism. *Environ. Sci. Technol.* **2006**, *40*, 6151–6156.
32. Kaindl, G.; Schmiester, G.; Sampathkumaran, E.; Wachter, P. Pressure-Induced Changes in L_{III} X-ray-Absorption Near-Edge Structure of CeO_2 and CeF_4: Relevance to 4f-Electronic Structure. *Phys. Rev. B.* **1988**, *38*, 10174.
33. Bianconi, A.; Marcelli, A.; Dexpert, H.; Karnatak, R.; Kotani, A.; Jo, T.; Petiau, J. Specific Intermediate-Valence State of Insulating 4f Compounds Detected by L_3 X-ray Absorption. *Phys. Rev. B.* **1987**, *35*, 806.
34. Zhang, Z.; Wang, Y.; Li, F.; Xiao, H.; Chai, Z. Distribution Characteristics of Rare Earth Elements in Plants from a Rare Earth Ore Area. *J. Radioanal. Nucl. Chem.* **2002**, *252*, 461–465.
35. Lissner, J.; Mendelssohn, I. A.; Anastasiou, C. J. A Method for Cultivating Plants under Controlled Redox Intensities in Hydroponics. *Aquat. Bot.* **2003**, *76*, 93–108.
36. Ndon, U.; Randall, A.; Khouri, T. Reductive Dechlorination of Tetrachloroethylene by Soil Sulfate-Reducing Microbes under Various Electron Donor Conditions. *Environ. Monit. Assess.* **2000**, *60*, 329–336.
37. Xia, T.; Kovochich, M.; Liong, M.; Mädler, L.; Gilbert, B.; Shi, H.; Yeh, J. I.; Zink, J. I.; Nel, A. E. Comparison of the Mechanism of Toxicity of Zinc Oxide and Cerium Oxide Nanoparticles Based on Dissolution and Oxidative Stress Properties. *ACS Nano* **2008**, *2*, 2121–2134.
38. Cervini-Silva, J.; Fowle, D. A.; Banfield, J. Biogenic Dissolution of a Soil Cerium-Phosphate Mineral. *Am. J. Sci.* **2005**, *305*, 711–726.